AIDA

Advanced European Infrastructures for Detectors at Accelerators

Conference Contribution

Demonstrator of the Belle II Online Tracking and Pixel

Bilka, T (OEAW) *et al*

19 June 2014

The research leading to these results has received funding from the European Commission under the FP7 Research Infrastructures project AIDA, grant agreement no. 262025.

This work is part of AIDA Work Package **9: Advanced infrastructures for detector R&D**.

The electronic version of this AIDA Publication is available via the AIDA web site <http://cern.ch/aida> or on the CERN Document Server at the following URL: <http://cds.cern.ch/search?p=AIDA-CONF-2015-013>

Demonstrator of the Belle II Online Tracking and Pixel Data Reduction on the High Level Trigger System

T. Bilka, G. Casarosa, R. Frühwirth, C. Kleinwort, P. Kodys, P. Kvasnicka, J. Lettenbichler, E. Paoloni, J. Rauch, T. Schlüter, S. Yashchenko

***Abstract*—We present a computer-farm based data reduction system for the pixel detector of the future Belle II experiment. Belle II is a major upgrade of the Belle detector that is currently ongoing in KEK (Tsukuba, Japan). Belle II will collect data from SuperKEKB, an asymmetric e^+e^- collider whose target luminosity ($8\cdot10^{35}$ Hz/cm^2) is a factor 40 larger than the present world record held by its predecessor KEKB. The higher trigger rate (10 kHz) and worse background conditions (3% average occupancy on the pixel sensors) are a major challenge for both the detectors and the Data Acquisition System (DAQ), in particular for the inner part of the Belle II tracking system that consists of two cylindrical layers of DEPFET pixels sensors (PXD) placed just outside the beam pipe and very close to the Interaction Point (IP). The long integration times of the PXD together with the high background rate expected from pair production occurring at the IP will lead to a large amount of data (more than 20 GB/s) that must be reduced by at least a factor 10 to satisfy the constraints coming from the available storage space and bandwidth. A large amount of the background hits can be rejected by defining a set of Region Of Interest (ROI) on the PXD sensors and then recording just the data from the pixels inside the ROI. The ROIs are defined on an event by event basis by extrapolating back onto the PXD the charged tracks detected in the outer silicon tracker (a 4 layer double-sided silicon strip detector) and reconstructed online in real time. A demonstrator of this architecture was under beam test earlier this year in DESY (Hamburg, Germany). The demonstrator was operated in an electron beam whose momentum was in the 2 - 6 GeV/*c* range with a typical trigger rate of a few kHz in a magnetic field of strength up to 1 T. The demonstrator consists of one PXD sensor and 4 SVD sensors arranged in a 5 layers configuration mimicking the Belle II vertex detector. The detector readout was a scaled down version of the full Belle II DAQ + High Level Trigger (HLT) chain. The demonstrator was used to detect the particles, reconstruct in real time the trajectories, identify the ROIs on the PXD plane and record the PXD data within. In this contribution, we describe the requirements and the architecture of the final system together with the results obtained with the demonstrator.**

I. Introduction

Manuscript received June 16, 2014.

T. Bilka, P. Kvasnicka and P. Kodys are with Faculty of Mathematics and Physics, Charles University in Prague, Czech Republic

R. Frühwirth and J. Lettenbichler are with HEPHY Vienna, Austria. J.L. is supported by the Austrian Science Fund (FWF), project P24182-N16.

C. Kleinwort and S. Yashchenko are with DESY, Hamburg, Germany

E. Paoloni and G. Casarosa are with INFN and the University of Pisa, Italy

J. Rauch is with Technische Universität München, Germany

T. Schlüter is with Ludwig-Maximilians-Universität München, Germany and Excellence Cluster Universe, Technische Universität München, Garching, Germany

THE Belle II experiment is a particle physics experiment currently being set up at the site of the High Energy Accelerator Research Organization (KEK) in Tsukuba, Japan, and will take its first physics data in 2016. It will exploit the unprecedented luminosity ($8 \times 10^{35}\,\mathrm{Hz/cm^2}$) of the SuperKEKB accelerator. The accelerator is an asymmetric e^+-e^- accelerator whose center-of-mass energy $\sqrt{s} = 10.58\,\mathrm{GeV}$ is the mass of the $\Upsilon(4S)$ resonance which will thus be produced in copious amounts. It almost exclusively decays into pairs of a B-meson and its antiparticle, no other decay could be established at a level above 10^{-4} [1]. This well-defined initial state $B\bar{B}$ can then be exploited for high-precision studies into flavor physics, the study of how the different types of quarks relate to each other and interact in the weak interaction. In the mathematical formulation of the Standard Model (SM) of particle physics, flavor physics finds its place in the Cabibbo-Kobayashi-Maskawa matrix, whose numerical values encode the wealth of phenomena. This matrix is also the only source of CP-violation in the SM, and as such, it is the only place where our current theory can try to explain the preponderance of matter over antimatter in Nature. High-precision studies of flavour physics are therefore essential to understanding why we exist.

Many existing studies from B-factories are limited by statistics, not systematics. For these measurements larger data sets are desirable. Sensitivity studies show a typical improvement of measurements by an order of magnitude if the integrated luminosity is increased from Belle's $0.5\,\mathrm{ab}^{-1}$ to $50\,\mathrm{ab}^{-1}$ at Belle II [2]. Collecting the huge amount of data required for precision physics poses a number of challenges that must be overcome in the experiment. First, the accelerator needs to provide high luminosity reliably. The instant luminosity aim for SuperKEKB exceeds that achieved by the predecessor accelerator KEKB by a factor of forty. The concurrent increase in physics data leads to a similar increase in the amount of data read out, subject to specific choices of triggers. The increase in luminosity is achieved on the one hand by roughly doubling the beam currents, on the other hand by a novel nano-beam scheme which leads to a beam size of order $10\,\mu\mathrm{m} \times 60\,\mathrm{nm}$ at the interaction point. The increased beam current and the more delicate optics lead to increased background levels in the detectors which are situated close to the beam line, the second challenge. These have to be dealt with at the high trigger rates foreseen.

One of the main avenues for studying CP-violating pro-

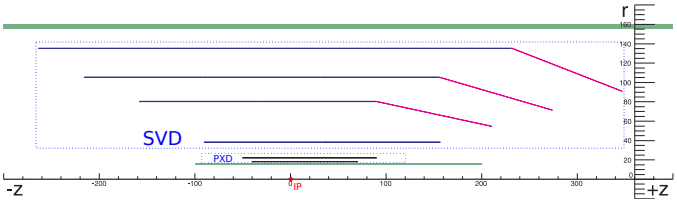

Fig. 1. Layout of the Belle II vertex detector (VXD). Distances in mm relative to the interaction point (IP) are indicated. The two layers of the pixel detector (PXD) and the four layers of the silicon vertex detector (SVD) are indicated. The VXD volume is bounded by the beam pipe on the inside and by the inner wall of the drift chamber on the outside (both indicated in green).

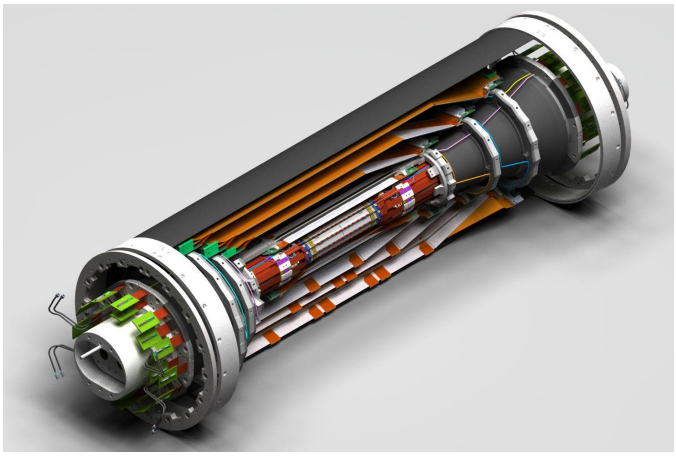

Fig. 2. Illustration of the full vertex detector setup. Reader-facing parts of the detector have been removed for visibility.

cesses is the study of flavor oscillations. These studies require precise time-of-flight measurement of the B and $\bar{B}$ mesons before their respective decays. Here, the relevant observable is the displacement between the points of decay ("vertices") of the B and $\bar{B}$ mesons subsequent to a typical $\Upsilon(4S)$ decay. To achieve utmost precision in this measurement, a high resolution detector for charged particles has to be installed as close as possible to the interaction point. In the Belle II experiment, this Vertex Detector (VXD) is composed of six layers of semiconductor detectors arranged in concentrical rings about the beam pipe. The two innermost layers (PXD) of this detector consist of DEPFET-type pixel sensors [3], situated at radii of 14 mm and 22 mm from the beam line, respectively. The outer four layers (SVD) consist of double-sided silicon strip detectors [4], situated at radii ranging from 38 mm to 140 mm from the beam line. In order to cover the full polar angular range of the remainder of the experiment, $17° < \vartheta < 150°$, the outer three layers use a wedged geometry in the forward direction, thus significantly reducing the necessary amount of silicon. The VXD is surrounded by a large drift chamber (CDC) used for precise momentum determination of charged particle tracks and particle identification by energy loss measurements. Further detectors for particle identification and neutral particle detection surround this ensemble of tracking detectors. The layout of the VXD is shown in Fig. 1 and 2.

Due to the proximity of the VXD, and especially the PXD, to the beam line, sophisticated background rejection has to be employed. Given the expected average occupancy of the PXD of 3%, the amount of data would be overwhelming, exceeding 20 Gb/s of raw pixel data. Background suppression therefore has to take place before storing data to disk. Additionally, the readout of the PXD requires an integration time of 20 μs which is only a factor 5 below the average spacing of two triggered events at the expected trigger rate of 10 kHz [2]. Therefore, hits from two different events triggered in close succession have to be correctly associated to the respective events.

In order to achieve these objectives, the High-Level Trigger (HLT) of Belle II performs online track finding and fitting in the SVD and the CDC, extrapolates the resulting tracks back to the PXD, and defines Regions-of-Interest (ROIs) based on the intersections of these tracks with the PXD surfaces. Data contained in these ROIs is then read out and stored for offline processing. In parallel, the data-merging hardware performs track-reconstruction and ROI definition in an FPGA-based approach.

A number of other contributions at this conference dealt with other parts of the Belle II DAQ. The global picture of the Belle II DAQ system is given in S. Yamada's contribution OS 1-1; the ONSEN system is discussed in more detail in T. Geßler's contribution PS 3-1; the event-building process is explained in S.Y. Suzuki's contribution PS 3-56; the design and implementation of the digitization and readout hardware of the PXD is detailed in D. Levit's contribution PS 3-20; R. Itoh's contribution PFS 2 discusses more of the data processing.

In this contribution, the design and implementation of the software used in the online reconstruction of the HLT system and the results we obtained in a test beam experiment which took place in January of 2014 are discussed. In this experiment, a sector of the VXD was exposed to an electron beam at DESY, and for the first time the whole system of PXD and SVD was successfully integrated with the Belle II DAQ system. The processing chain including the above-mentioned online reconstruction could be established during the test beam experiment. Additionally, the detector was operated in a cooled environment, and slow control was handled with the slow control system foreseen for the final experiment.

II. Experimental Setup

The demonstrator was operated in an electron beam at DESY. The average beam momentum was in the $2-6\,\mathrm{GeV}/c$ range with a typical beam rate of a few kHz. The beam passed through the coil of a solenoid magnet (1 T) inside of which the detector assembly was installed. Bremsstrahlung processes in the magnet solenoid lead to a broad momentum distribution of the particles entering the detector volume. A side view illustrating the detector positions and measurements is shown in Fig. 3.

Unlike the final experiment, only one PXD layer (corresponding to PXD2 in the figure) was installed. It contains a matrix of 480×192 pixels of $75 \times 50\,\mu\mathrm{m}^2$ each and is thinned down to 50 μm. As in the final experiment, the long side is parallel to the magnetic field. The detector is orthogonal to the nominal beam direction, the bending direction is therefore along the short side of the detector. Its digitization and readout

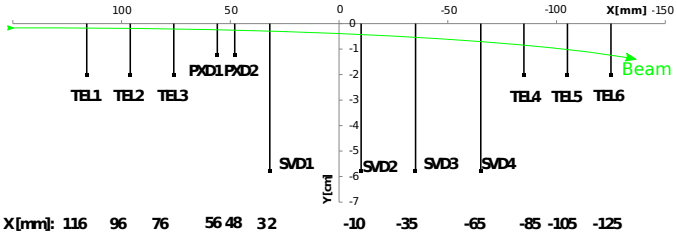

Fig. 3. Experimental setup in the test beam experiment. The beam (green) enters from the left where it transverses the coil of the solenoid magnet before reaching the experiment. There it passes through three planes of the EUDET beam telescope [5]. These are followed by the VXD planes in a setup mimicing a sector of the final Belle II assembly: first two layers of DEPFET pixel detectors (PXD1-2), then four planes of double-sided silicon strip detectors (SVD1-4). Finally, three additional telescope layers for exact position determination. The PXD1 plane was not present.

ASICs are as close as possible to the final specifications for the Belle II experiment, but in the final experiment the detectors will be 75 μm thick. A second sensor of the final specifications could not be prepared in time. Nevertheless, this setup allowed exercising the complete readout and processing chain with real data.

Downstream of the PXD layers, four SVD layers were installed. The first layer had an active area of $123 \times 38\,\mathrm{mm}^2$ and a thickness of 320 μm. The detector had 768×512 strips, with pitches of 160 μm and 75 μm respectively. It was oriented in the same manner as the PXD layer. The other three SVD layers had the same specifications, but 768×768 strips and a corresponding active area of $123 \times 58\,\mathrm{mm}^2$. The detector layers employed were subject to previous tests of radiation hardness. This lead to localized hot areas. These were masked during clusterization.

The VXD assembly was contained inside a dry volume cooled with CO_2. Cooling as well as detector power supply slow control was using the final Belle II software. The cold volume is placed between the two arms of the EUDET beam telescope [5] provided by the test beam facility. It was used for alignment purposes and efficiency studies. The system was triggered by a coincidence between two pairs of scintillators placed in front and behind the assembly, respectively. The telescope data was recorded along a separate data path and merged offline. See Fig. 4 for a detailed view of the readout. We highlight a few details of the architecture in the following.

Once the Trigger Logic Unit (TLU) found a coincidence between the scintillators, it assigned an event number and sent it together with a trigger signal to the telescope readout (bottom left) and the Frontend Timing Switch (FTSW). This in turn triggered readout of the SVD by the Pocket DAQ (top left) which was a scaled down version of the common DAQ used by all Belle II detectors save the PXD. Once the data were collected and an event built, it was sent to the High Level Trigger (HLT, top right) whose operation will be discussed in detail below. Continuing with the PXD readout (middle left), upon receiving a trigger from the FTSW, the DHHC ASIC forwarded data integrated by the PXD to the Online Selector Node (ONSEN) which has sufficient memory to store several seconds of data under typical conditions in the Belle II experiment. Besides buffering, the ONSEN system was responsible

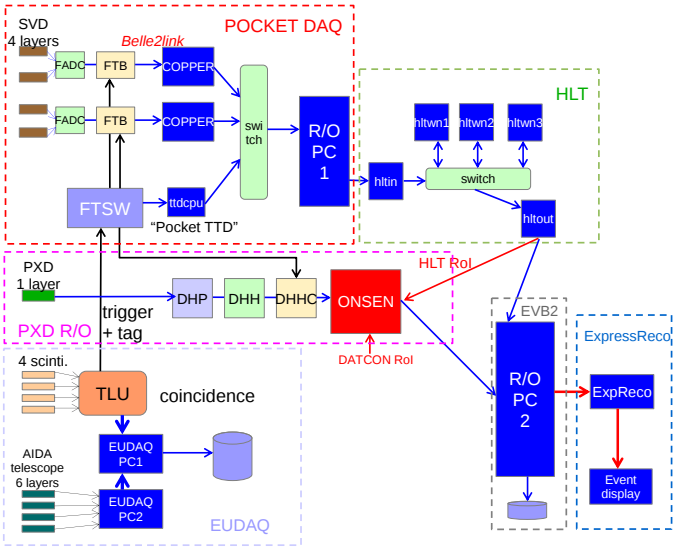

Fig. 4. Block diagram of the readout of the DESY test beam experiment. The software described in this contribution resides in the boxes labelled HLT and ExpressReco. SVD data collected by R/O PC 1 is forwarded to the HLT. Here, several PCs process data with event-wise parallelism. The resultant data are forwarded to the second-stage event building EVB2. At the same time the HLT sends ROIs to the ONSEN system which in turn forwards the pixel data contained in these ROIs to EVB2. There the events are merged and stored to disk. For monitoring purposes, events are also sent to the ExpressReco system, which performs a reconstruction including all layers. (Figure courtesy of R. Itoh.)

for data reduction. It did so based on Regions of Interest (ROIs) defined in two ways: by the HLT (discussed below) or by an FPGA-based tracking implemented in hardware (DATCON, not depicted). The pixel data corresponding to these ROIs was forwarded to the second event builder (bottom right) where it was merged with the SVD data received from the HLT. The data was then stored to disk, and a fraction of the events was forwarded to the ExpressReco, a fast reconstruction with the purpose of data quality inspection. This operation matched the data paths foreseen in the Belle II experiment.

III. Requirements

In the test beam experiment, the following requirements had to be met by the HLT software:

1) reading of detector data formats;
2) efficient track finding and fitting;
3) extrapolation of tracks to PXD planes;
4) definition of ROIs;
5) successful communication of ROIs to the ONSEN systems.

The HLT system consisted of five computing nodes in total. Two twelve-core systems (hltin and hltout) handled the event-wise data distribution to the HLT worker nodes (hltwn1-3) which were 24-core systems.

The data distribution and processing was implemented in the Belle II software framework, `basf2` [6], [7]. This framework has a modular architecture, where individual data processing steps are implemented in a chain of independent modules which can be implemented in the C++ or Python programming languages. The processing of this chain is managed by small

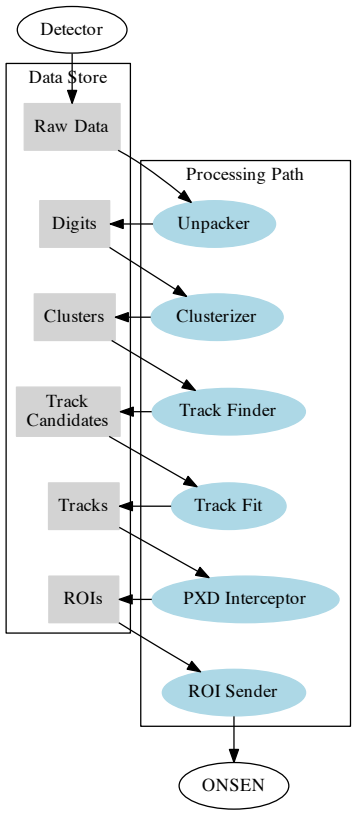

Fig. 5. Block diagram of the data processing in the HLT. The sequence of modules in the processing path is traversed in order. Each processing module is indicated as a blue oval. Data store arrays (indicated as grey rectangles) as serve as input and output of the individual modules. Arrows indicate the direction of the data flow.

programs ("steering files") written in Python. The means of communication between the modules is the so-called datastore, which consists of named and typed arrays where modules can read and write data. Subsequent processing steps can read the datastore arrays provided by previous steps. The implementation is such that the datastore can be streamed to and from disk or over the network at any point in the processing chain. This way, processing tasks can be distributed over a network of computers or multiple processor cores with no further requirements on the implementation of individual steps. Likewise, processing can be stopped at every step, the results can be stored to disk, and further processing or reprocessing can happen at any time. The implemenation of the data store is based on the I/O facilities of the ROOT framework, a C++ library which is commonly used in particle physics [8]. Common configuration data such as the detector geometry is held in a database, which was implemented by XML files during the test beam.

IV. Data Processing Chain

A. Overview

The HLT implementation on the test beam consisted of the following processing path on each worker node (Fig. 5): the raw data were converted to digits by an unpacker for the SVD data format. It took care of the conversion of channel numbers to row and column numbers and it also masked hot areas of the detectors. In the next step, the digits were processed by clusterization algorithms. These combined the digits into clusters, evaluating the actual hit position while taking into account Lorentz corrections to electron drift in the presence of a magnetic field. The clusters form the actual input for the track finder, discussed below. The track finder outputs track candidates which in turn are fit with a Kalman fitter (discussed below) and the fitted tracks are used by the PXD Interceptor module to define the ROIs on the PXD. Once the processed event has arrived on the hltout node, it runs the ROI Sender module which takes care of the communication with the ONSEN system.

B. Track Finding

Tracks are found using an approach based on a cellular automaton (CA, [9]), where the combinatorial problem of finding track candidates is reduced by sequentially applied filters with increasing complexity. The central aspect of the CA and the first filter stage in the track finder (CA-TF) is the formation of track segments that combine compatible hits to cells. Cells sharing a hit are allowed to become neighbors if they fulfill certain geometrical requirements, for instance a cut on the angle between the cells; this is the second filter stage. Each cell is assigned a discrete state. The state of each cell evolves in discrete time steps by checking the local neighborhood. The maximum state of a cell is limited by the length of a chain of compatible cells along the track. Therefore cells are suitable for collecting track candidates (TCs). The TCs are assigned a quality indicator (QI) by a fast fit of a circle to the trajectory in the bending plane. To determine a final set of non-overlapping TCs, the QIs are used by a Hopfield network to determine the best set. During filtering a trade-off between rejecting as many bad combinations as possible while retaining as many good combinations as possible has to be made. To ensure the physically most relevant cutoffs, the output of extensive Monte Carlo-simulations is used to compute look-up-tables. These so-called sector-maps take the local position of the hits in the detector into account and are iteratively applied for different momentum ranges.

To determine the performance of the CA-TF, a reference set of tracks was determined in as follows. The data were scanned for events where the following conditions were met:

- there was at least one hit in the PXD;
- there was an existing (loose) correlation of hits between neighboring layers;
- the correlation had to be intact for the inner 3 telescope layers, the PXD and the SVD;
- the outer 3 telescope layers had to provide correlated hits too.

The surviving events were used for finding track candidates by creating all possible hit combinations and fitting the result. Only the best fit of an event was stored and used to measure the performance of the CA-TF. Since the combinatorial problem of combining at least 8+3 layers is very severe, the fit procedure

TABLE I
CONTINGENCY TABLE.

	no reference TC	reference TC
no TC from CA-TF	n_{00}	n_{10}
TC from CA-TF	n_{01}	n_{11}

TABLE II
SETTINGS OF THE TWO RUNS USED IN THE TRACK FINDING STUDIES.

run	field strength	beam energy	events
470	0T	3GeV	4687
510	1T	3GeV	10282

was aborted if it took too long. Therefore not all events fulfilling the conditions mentioned above provided reference TCs. As a consequence, events with many hits did not give a reference TC, although the CA-TF did. A straightforward definition of efficiency is misleading, therefore a closer look is necessary. It should be kept in mind that for the purposes of the high-level trigger, the CA-TF uses only hits in the SVD to find track candidates.

For a given run, a contingency table as shown in Table I can be created. The sum n_{tot} of all elements in the table is equal to the number of events in the run. The table can be used to define a measure of efficiency of the CA-TF. To cover several aspects two different types of efficiency were used to benchmark the TF performance:

1) the fraction of events where either both a reference TC was present and the CA-TF found a TC or where no TCs could be found:
$$\epsilon_1 = \frac{n_{00} + n_{11}}{n_{\text{tot}}};$$
2) number of events where the CA-TF found a TC (no matter whether the reference found a track too), divided by the total number of events where a TC was found by either approach:
$$\epsilon_2 = \frac{n_{01} + n_{11}}{n_{\text{tot}} - n_{00}}.$$

The first definition ϵ_1 would be appropriate if the reference could have found TCs in high occupancy events too. But since this would have been too time-consuming, that approach discards many good candidates provided by the CA-TF and therefore overestimates the number of bad cases. The second definition ϵ_2 ignores cases when the reference failed to find TCs and uses the reference only to find events which can be excluded from the total number of events.

The TF was tested in two different settings; first, a run without magnetic field, which allows checks for high occupancy cases since secondaries created by passing through the magnetic coil are not deflected by the magnetic field; second, a run with a field of 1T to test the behavior under more realistic conditions. Table II gives an overview over the settings used for the chosen runs.

The frequency distributions of the average number of hits per layer in the SVD are show in Figs. 6 and 7 for runs 470 and 510, respectively. Taking the average over the layers as a rough benchmark, run 470 provided an average number of about 1100 possible hit combinations per event. Many secondaries

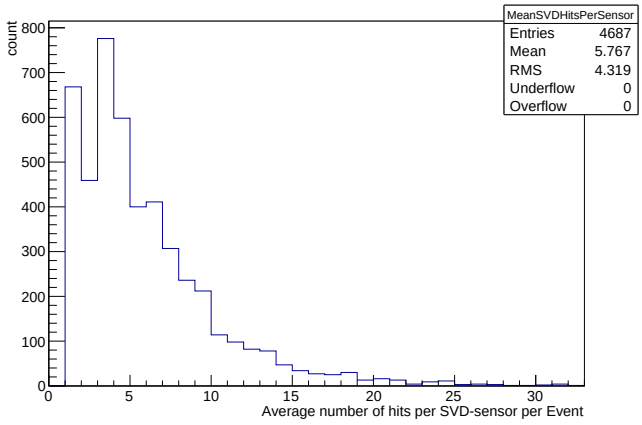

Fig. 6. Average number of hits per layer, run 470 (no magnetic field).

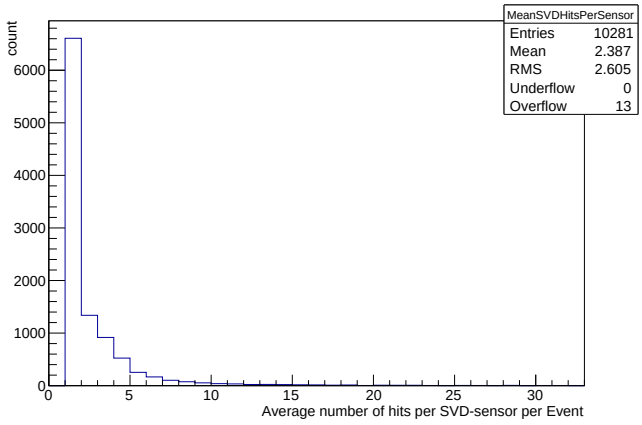

Fig. 7. Average number of hits per layer, run 510 (1 T magnetic field).

produce a high rate of ghost hits. This background is a good test for high track multiplicity. Run 510 provided an average number of only 32 possible combinations per event. As the magnetic field deflects low momentum secondaries, this run is much cleaner than the other one. This has a major impact on the execution time per event. Since the trigger rate was about 1kHz and 24 cores were used in the HLT-demonstrator, the total time budget for each event was about 40 ms. To leave enough room for other modules such as fitting and ROI finding, the TF should use only 10% of the given budget, or 4 ms. The speed of the CA-TF is mainly limited by the total number of *accepted* hit combinations per event, i.e., the ones that are used as cells in the CA. To test the behavior of the CA-TF the chosen runs were analyzed with the following thresholds on the number of cells: 1250, 1000, 750, 500, 250, 125, 65. Events exceeding the threshold are skipped. In Fig. 8, the performance of the CA-TF is plotted as function of execution time per event for both runs. Using the highest threshold results in the best efficiencies but requires the longest execution time per event. While run 510 can be analyzed with the highest threshold within the timing constraints, for run 470 the limit should be set to about 1000 in order to stay below the limit of 4 ms. In both runs the CA-TF found TCs

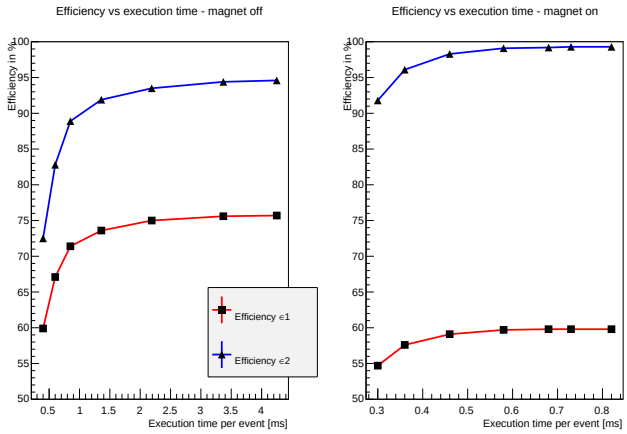

Fig. 8. Left: run470, right: run510. Runs were analyzed using different thresholds (low: fast, high: slow) for the number of accepted hit combinations (cells).

much more often than the reference, which can be partially explained by the terminating condition for high occupancy cases with the reference procedure. In the run with activated magnetic field the effect of high occupancy is less dominating. Actually, much fewer reference TCs were generated because the downstream telescope sensors (not requird by the CA-TF) were not hit by particles that lost a significant fraction of their momentum before entering the detector volume (see Fig. 9).

C. Track Fitting

The hit combinations together with an initial momentum estimate are stored as track candidates. These are then processed with a version of the GENFIT track fitting software [10]. This track fitting package has been largely overhauled to meet the requirements of the Belle II experiment. GENFIT implements a flexible framework for the modelling, extrapolating and fitting of charged-particle trajectories in complex detector environments. For the purposes of definition of ROIs, the track candidates are fitted with the standard Kalman fitter algorithm [11]. For the purposes of detector alignment the Generalized Broken Lines (GBL) [12] algorithm is employed offline. Another track fitting algorithm implemented in GENFIT is the Deterministic Annealing Filter. This is the standard algorithm used in Belle II. The average time for the fit of a single track in the current experimental setup was < 1 ms on a typical laptop. Computing time requirements of the HLT were thus easily fulfilled. In Fig. 9 reconstructed momentum spectra for runs with three different beam momentum settings are shown.

D. Determination of Regions of Interest

Once tracks are fitted based on hits in the SVD planes, the definition of the regions of interest (ROIs) takes place. These are defined by areas on the PXD planes which are likely to have been crossed by the fitted tracks. Once the ROIs are determined by the HLT, they are forwarded to the Online Selector Node system (ONSEN) which holds the PXD data until requested, and the ONSEN system in turn

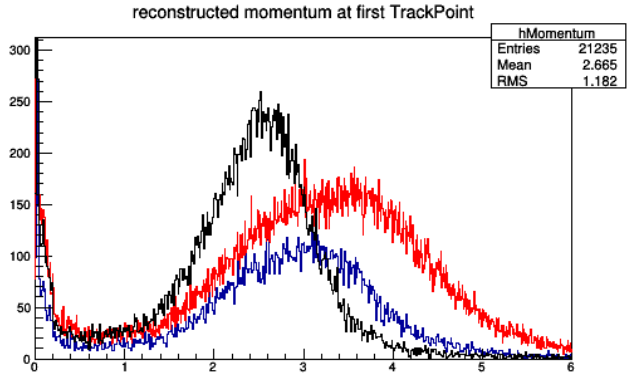

Fig. 9. Measured momenta in GeV with three different beam settings. The curves are scaled to clearly separate the curves. The momentum spread is due to bremsstrahlung energy losses of the electrons while passing through the solenoid magnet. Low-momentum tracks are bent away from the detector planes.

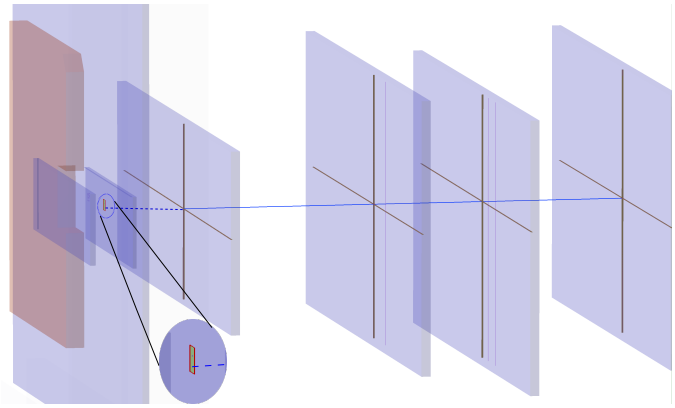

Fig. 10. Illustration of the ROI definition process. A track (blue, enters from the left) is fitted through the hits on the four SVD planes (four rightmost light blue planes). Based on the backwards extrapolation (dotted blue) to the PXD plane, the ROI is defined (area with red boundary). Indeed a hit is found within this area. The area surrounding the ROI is shown enlarged in the inset.

forwards the PXD data contained within the ROIs to the second event builder (EVB2). Here the pixel data is merged with the SVD data (and the data from the other detectors in the full experiment) in order to assemble the complete events which are then stored to disk.

The ROIs are found by the following procedure:

1) Find intercepts of all fitted tracks with the PXD planes.
2) Define rectangular arrays of pixels surrounding the intercept. The size of the array is determined by both the extrapolation errors and an allowance for systematic errors such as misalignment.

A high efficiency of the ROI determination is observed, leading to a more than twenty-fold reduction of the amount of PXD data. Communication of the ROIs to the ONSEN system could be established, both transferring artificial ROIs (full detector plane, patterns) and real ROIs determined in the above manner. The procedure is illustrated for an example event in Fig. 10. A distribution of two-dimensional offsets between the measured pixel hits and the calculated intercepts is shown in Fig. 11.

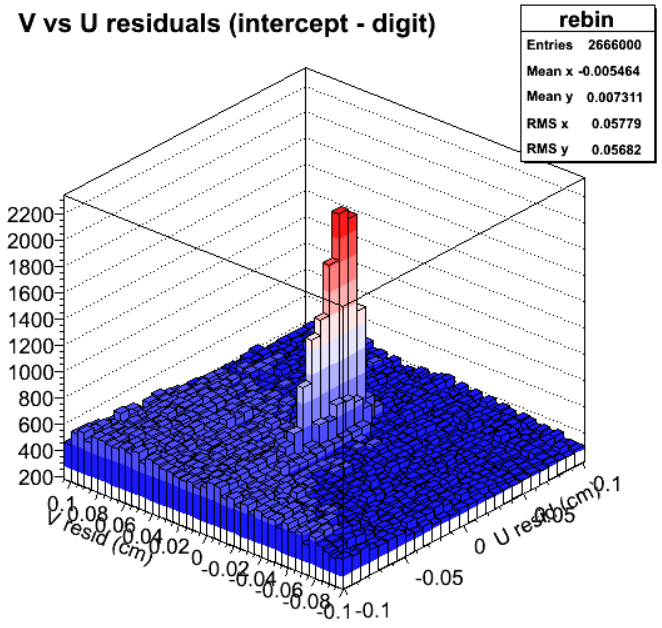

Fig. 11. Residual between the intercept of the reconstructed SVD-track on the PXD plane and the actual PXD hits for 1 000 000 test beam events. The bins match the PXD pixels. A Gaussian fit estimates the width of the central peak as $(32.3 \pm 0.4)\,\mu$m and $(141 \pm 2)\,\mu$m in the V and U directions, respectively. Here U denotes the bending direction.

E. Alignment

For the purpose of alignment of the detector setup, the default alignment procedure developed for the Belle II vertex detector which is fully integrated to the Belle II software is applied. The procedure utilizes the Millepede II algorithm described in Ref. [13]. Data for Millepede II are prepared by a refit of reference tracks (provided by the track finder) using General Broken Lines (GBL) [**?**] integrated into the GENFIT package to take advantage of its extrapolation capabilities. In GBL, multiple scattering is taken into account representing thick scatterers by two equivalent thin scatterers at detector planes and in between.

The alignment procedure is successfully applied for data obtained with and without magnetic field. Alignment corrections determined for sensor displacements and rotations in their planes have typical uncertainties below $3\,\mu m$ / $0.5\,$mrad and differ usually by less than 1 mm / 10 mrad from the nominal geometry. The only exception is the PXD sensor shifted by about 5mm. In Fig. 12 change of residual distributions after alignment of the second SVD sensor in the magnetic field is presented. Clear improvements of residuals after the alignment procedure are observed.

V. Summary

During the test beam campaign which concluded in January 2014 the readout and data reduction scheme of the Belle II vertex detector could be proven. A number of milestones were achieved:

1) simultaneous operation of SVD and PXD detectors;
2) common readout of all subsystems with the final Belle II architecture;

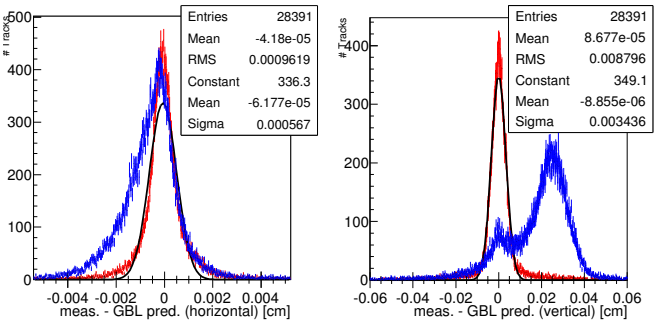

Fig. 12. GBL refit residuals in V (left) and U (right) directions of the second SVD sensor using nominal (blue) and aligned (red) geometry. Parameters of a Gaussian fit (black curve) to the red histogram are given.

3) online, real-time processing of SVD data with the full reconstruction software also used for offline;
4) usage of the Belle II software framework's network data distribution and parallel processing capabilities;
5) cellular automaton based track finding;
6) readout of the PXD could be successfully be driven by the SVD data;
7) processing steps such as alignment could successfully be performed.

Acknowledgment

This work would not have been possible without hard work by the Belle II PXD, SVD and DAQ test beam teams, led by C. Marinas, C. Irmler and R. Itoh, respectively, nor would it have been possible without the DESY test beam facilities. This research was supported by the DFG cluster of excellence 'Origin and Structure of the Universe', by the Ministry of Education, Youth and Sports of the Czech Republic under Contract No. LG14034, and by the Austrian Science Fund (FWF), project P24182-N16. The research leading to these results has received funding from the European Commission under the FP7 Research Infrastructures project AIDA, grant agreement no. 262025.

References

[1] J. Beringer *et al.*, "Review of Particle Physics (RPP)," *Phys.Rev.*, vol. D86, p. 010001, 2012.
[2] T. Abe *et al.*, "Belle II Technical Design Report," 2010.
[3] O. Alonso *et al.*, "DEPFET active pixel detectors for a future linear e^+e^- collider," *IEEE Transactions on Nuclear Science*, vol. 60, no. 2, pp. 1457–1465, April 2013.
[4] M. Friedl, K. Ackermann, H. Aihara, T. Aziz, T. Bergauer *et al.*, "The Belle II Silicon Vertex Detector," *Nucl.Instrum.Meth.*, vol. A732, pp. 83–86, 2013.
[5] A. Bulgheroni, "Results from the EUDET telescope with high resolution planes," *Nucl.Instrum.Meth.*, vol. A623, pp. 399–401, 2010.
[6] R. Itoh, S. Lee, N. Katayama, S. Mineo, A. Moll *et al.*, "Implementation of parallel processing in the basf2 framework for Belle II," *J.Phys.Conf.Ser.*, vol. 396, p. 022026, 2012.
[7] S. Lee, R. Itoh, N. Katayama, and S. Mineo, "Development of high level trigger software for Belle II at SuperKEKB," *J.Phys.Conf.Ser.*, vol. 331, p. 022015, 2011.
[8] R. Brun and F. Rademakers, "ROOT: An object oriented data analysis framework," *Nucl.Instrum.Meth.*, vol. A389, pp. 81–86, 1997.
[9] R. Frühwirth, R. Glattauer, J. Lettenbichler, W. Mitaroff, and M. Nadler, "Track finding in silicon trackers with a small number of layers," *Nucl.Instrum.Meth.*, vol. A732, pp. 95–98, 2013.

[10] C. Höppner, S. Neubert, B. Ketzer, and S. Paul, "A Novel Generic Framework for Track Fitting in Complex Detector Systems," *Nucl.Instrum.Meth.*, vol. A620, pp. 518–525, 2010.
[11] R. Frühwirth, "Application of Kalman filtering to track and vertex fitting," *Nucl.Instrum.Meth.*, vol. A262, pp. 444–450, 1987.
[12] C. Kleinwort, "General Broken Lines as advanced track fitting method," *Nucl.Instrum.Meth.*, vol. A673, pp. 107–110, 2012.
[13] V. Blobel, "Software alignment for tracking detectors," *Nucl.Instrum.Meth.*, vol. A566, pp. 5–13, 2006.